An Altered Mode of Calcium Coordination in Methionine-Oxidized Calmodulin

Eric M. Jones, Thomas C. Squier, and Colette A. Sacksteder
Cell Biology and Biochemistry Group, Biological Sciences Division, Fundamental and Computational Sciences Directorate, Pacific Northwest National Laboratory, Richland, Washington 99352

ABSTRACT Oxidation of methionine residues in calmodulin (CaM) lowers the affinity for calcium and results in an inability to activate target proteins fully. To evaluate the structural consequences of CaM oxidation, we used infrared difference spectroscopy to identify oxidation-dependent effects on protein conformation and calcium liganding. Oxidation-induced changes include an increase in hydration of α-helices, as indicated in the downshift of the amide I′ band of both apo-CaM and Ca^{2+}-CaM, and a modification of calcium liganding by carboxylate side chains, reflected in antisymmetric carboxylate band shifts. Changes in carboxylate ligands are consistent with the model we propose: an Asp at position 1 of the EF-loop experiences diminished hydrogen bonding with the polypeptide backbone, an Asp at position 3 forms a bidentate coordination of calcium, and an Asp at position 5 forms a pseudobridging coordination with a calcium-bound water molecule. The bidentate coordination of calcium by conserved glutamates is unaffected by oxidation. The observed changes in calcium ligation are discussed in terms of the placement of methionine side chains relative to the calcium-binding sites, suggesting that varying sensitivities of binding sites to oxidation may underlie the loss of CaM function upon oxidation.

INTRODUCTION

Calmodulin (CaM), the ubiquitous Ca^{2+}-binding regulatory protein of eukaryotes, is the chief mediator of Ca^{2+}-dependent signaling events in the cell (1,2). In response to rises in intracellular Ca^{2+} levels, CaM binds up to four Ca^{2+} ions and undergoes a marked conformational change, enabling the protein to recognize and bind a multitude of target proteins and to reorganize its distribution among Ca^{2+}-dependent versus Ca^{2+}-independent binding partners (1–3). Among the targets activated by CaM are metabolic enzymes, kinases and phosphatases, ion channels, and transcription factors, which places CaM in a pivotal ''switch'' role in such cellular processes as inflammatory response, transcription, and synaptic potentiation (2,3).

Calmodulin shares many structural features with other small Ca^{2+}-binding proteins such as troponin C, calbindin, and recoverin (4). Calmodulin contains four canonical EF-hand Ca^{2+} binding motifs, which exist as pairs in the N-terminal and C-terminal lobes separated by a metastable linker sequence (5–10). EF-hands are helix-loop-helix structures that were named using traditional helix nomenclature for the protein albumin and represent a common binding motif for calcium (86). Cooperative binding of four Ca^{2+} ions to the four EF-hands stabilizes an elongated CaM structure, in which the hydrophobic target-binding surfaces are exposed on either lobe (7). The utility of CaM as a signaling protein, therefore, depends on its ability to structurally couple Ca^{2+} binding with target protein recognition. Disrupting either of these events, or their physical linkage, can compromise or abolish CaM function.

Although pathological CaM mutations are rare (CaM has an identical sequence in all vertebrates), covalent posttranslational modifications of CaM are common, and modulate the Ca^{2+} binding affinity and extent of fractional activation of target proteins (11–15). One such modification is the oxidation of methionine residues by reactive oxygen species, which generate methionine sulfoxide (MetSO) to form oxidized CaM (CaM_{ox}). Oxidation of the critical Met residues, Met^{144} and Met^{145}, to MetSO greatly reduces the ability of CaM to activate target proteins (11,15–20), and decreases the protein's affinity for Ca^{2+} (21–24). Oxidation of CaM methionines in vivo was suggested to serve as a means of dampening Ca^{2+} signaling in response to prolonged stress, aging, or physical insults such as ionizing radiation (11,25,26). In this respect, ionizing radiation generates large amounts of reactive oxygen species in cells (27) and mobilizes Ca^{2+}-dependent responses, of which CaM is an integral part (25,28). Oxidation of CaM methionines, therefore, may provide a means of ''cross-talk'' between the oxidative and cell-signaling effects of radiation exposure.

The structural mechanism underlying the effects of Met oxidation on CaM function, however, remains uncertain. It was suggested that Met oxidation results in global conformational changes that disrupt the helical structure of apo-CaM, interfering with the ability of CaM_{ox} to bind all four Ca^{2+} ions and activate target proteins (23,29). Alternatively, oxidation may result in a more subtle conformational change that allows complete Ca^{2+} binding, but selectively alters Ca^{2+} liganding to diminish the binding affinity. This possi-

Submitted June 18, 2008, and accepted for publication August 5, 2008.

Address reprint requests to Colette A. Sacksteder, Cell Biology and Biochemistry Group, Biological Sciences Division, Fundamental and Computational Sciences Directorate, Pacific Northwest National Laboratory, PO Box 999, MSIN P7-56, Richland, WA 99352. Tel.: 509-376-1937; Fax: 509-372-1632; E-mail: colette.sacksteder@pnl.gov.

Editor: Feng Gai.

0006-3495/08/12/5268/13 $2.00

doi: 10.1529/biophysj.108.139634

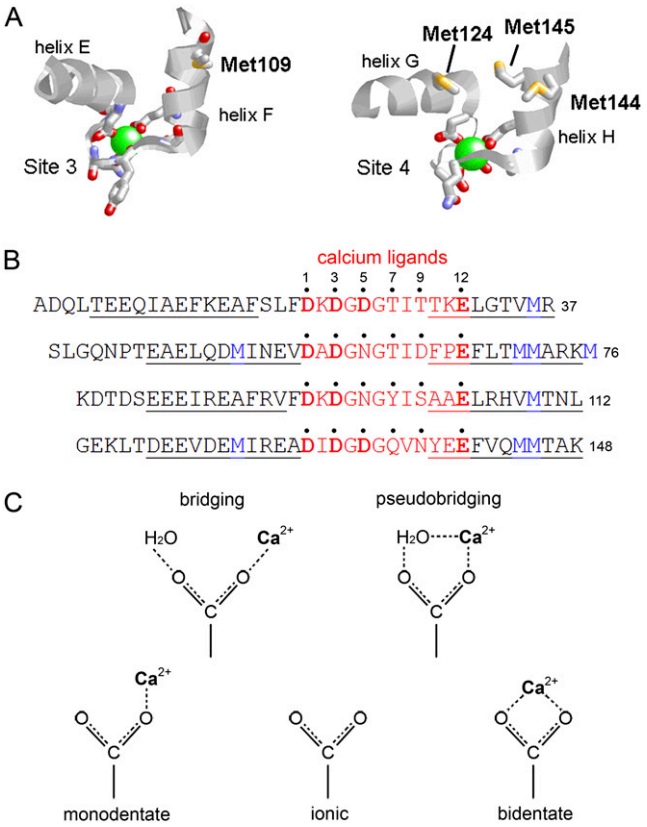

FIGURE 1 The EF-hand coordination of Ca^{2+} in CaM. (*A*) Structures of the third (*left*) and fourth (*right*) calcium-binding sites of CaM (7) (Protein Data Bank code 1cll), indicating the position and orientation of Met residues with respect to calcium (*green*)-liganding groups. (*B*) Sequence alignment of 12 amino-acid Ca^{2+} binding sequences (*red*) in EF-hands of vertebrate CaM. Residues providing a calcium ligand are numbered and marked with a dot. Ligands at positions 7 and 9 in each EF-loop coordinate calcium through a backbone carbonyl or through a water molecule bound to the side chain, respectively. All other residues coordinate calcium directly via the side chain. Acidic residues (Asp or Glu), in which coordination occurs via the side-chain carboxylate group, are shown in boldface. The proximity of methionines (*blue*) is indicated, showing that all binding sites have at least one Met residue in equivalent positions in one of the helices that flank the EF-loop (helical sequences are underlined). (*C*) Nomenclature for carboxylate side-chain coordination geometries.

bility is supported by the proximity of methionine residues to Ca^{2+} ligands within the CaM structure (Fig. 1). Ca^{2+} binds to an EF-hand domain, which consists of a helix-loop-helix structure, where the majority of Ca^{2+} coordination residues are located in the EF-loop, and an additional residue is in the subsequent N-terminal helix (Fig. 1 *B*). Within the 12-residue binding sequence, highly conserved Asp and Glu side chains coordinate Ca^{2+} at Asp^{1}, Asp^{3}, Asp^{5} (or Asn^{5}), and Glu^{12} (4). All of these side chains coordinate Ca^{2+} through a single oxygen atom (i.e., monodentate coordination, Fig. 1 *C*), except for Glu^{12}, which binds in a bidentate mode. The coordination sphere is completed by a backbone amide carbonyl at position 7 and a water molecule stabilized by the side chain at position 9. The CaM sequence shows that all Ca^{2+}-binding sites have at least one Met residue in the C-terminal EF-hand α-helix, whereas Ca^{2+}-binding sites 2 and 4 have two, with an additional Met residue in the N-terminal helix (Fig. 1). A disruption of the EF-hand helices by the presence of MetSO has the potential to alter Ca^{2+} liganding.

To investigate the structural effects of Met oxidation on the conformation of CaM and how the liganding of Ca^{2+} is altered, we examined H_2O_2-oxidized and nonoxidized CaM in solution, using Fourier-transform infrared (FTIR) spectroscopy. An established technique for the determination of protein conformation (30–35), FTIR spectroscopy also exhibits exquisite sensitivity and an ability to monitor the structure of both the protein backbone and amino-acid side chains, making it ideal for rapid and simultaneous measurements of protein conformation and ligand binding (30,36–38). Particularly useful to our investigations is the demonstrated ability of FTIR spectroscopy to discriminate the different coordination modes (Fig. 1 *C*) of Glu or Asp side chains bound to metal ions (39–44). Our spectroscopic data provide evidence that Met oxidation increases solvent exposure of the α-helices of CaM, and modifies the coordination of Ca^{2+} by carboxylate side chains in the EF-loop. These findings support the view that the oxidation of CaM modifies its function primarily through disruption of tertiary contacts, and suggests that the loss of Ca^{2+} affinity upon oxidation is a direct result of a perturbation of Ca^{2+} binding sites.

EXPERIMENTAL PROCEDURES

Materials

Deuterium oxide (D_2O, 99.9 atom % D) was purchased from Aldrich Chemical Co. (Milwaukee, WI). Ethylene glycol-bis(2-aminoethylether)-*N,N,N′,N′*-tetraacetic acid (EGTA) was purchased from Fluka (Basel, Switzerland). All other buffers and chemicals were from Sigma (St. Louis, MO), were of reagent grade, and were used without additional purification.

Expression and purification of CaM

Recombinant vertebrate CaM was produced by expression in *Escherichia coli* from the pET15b expression vector, as described previously (17). Protein was purified by hydrophobic interaction chromatography on a phenyl-sepharose CL4B column, as described previously (45). Purity of all proteins was at least 95%, as determined from polyacrylamide gel electrophoresis (data not shown). Calmodulin was stored as a lyophilized powder at −20°C until use. In all experiments, the concentration of CaM was determined spectrophotometrically, using an extinction coefficient of 2980 M^{-1} cm^{-1} at 280 nm (calculated with the ProtParam tool on the ExPASy website, http://ca.expasy.org/tools/).

Oxidation of CaM methionine residues

Unless otherwise stated, the oxidation of CaM was performed as described previously (15). Briefly, lyophilized protein was dissolved to ~1 mg/mL in oxidation buffer (50 mM Tris-HCl, 120 mM KCl, 1 mM $MgCl_2$, 100 μM $CaCl_2$, pH 7.4), to which concentrated hydrogen peroxide (H_2O_2) was added to a final concentration of 50 mM. Oxidation was allowed to proceed at room temperature (23°C ± 1°C) for 24 h, and was stopped by passing the reaction volume through a 5-mL HiTrap desalting column (GE Healthcare, Uppsala, Sweden) containing Sephadex G25 and equilibrated with water. The void

volume (containing CaM_{ox}) was immediately frozen and lyophilized, and was used within 2 weeks of preparation. Under these reaction conditions, complete oxidation of all nine methionine residues of CaM occurs (15,17), as verified by observing the characteristic decrease in electrophoretic mobility of CaM_{ox} in the presence of 10 mM $CaCl_2$ (17,21) (data not shown). Infrared spectra showed that one cycle of freezing-lyophilization did not appreciably alter the secondary structure and conformation of CaM_{ox} (data not shown). The oxidation of CaM was further verified by the presence of a very weak band at 1035 cm^{-1} in transmission-mode spectra in D_2O (data not shown); sharp bands at 1030–1050 cm^{-1} in proteins were assigned to the S=O stretch vibration of MetSO (46).

Infrared spectroscopy

The CaM samples for FTIR spectroscopy were prepared by dissolving lyophilized protein in buffer at ~10 mg/mL (~600 μM). Samples in D_2O were allowed to equilibrate at room temperature for at least 18 h before use, to allow for complete exchange of amide protons. Unless specified otherwise, all buffers contained 20 mM Tris-HCl (pH/pD 7.5) and 120 mM KCl. Buffers for Ca^{2+}-CaM contained 10 mM $CaCl_2$. Samples of Mg^{2+}-CaM contained 150 mM $MgCl_2$ and no calcium salts. Before the addition of buffer, apo-CaM and Mg^{2+}-CaM samples were depleted of metals as follows: protein was diluted to ~2 mg/mL in a solution of 2 mM EGTA and 2 mM ethylenediaminetetraacetic acid (EDTA), and allowed to sit for 3 h at room temperature. The protein solution was then dialyzed exhaustively against MilliQ deionized water for 24 h at 4°C, and then frozen, lyophilized, and reconstituted in the appropriate buffer. Immediately before use, samples were passed through a sterile 0.2-μm polyvinylidene fluoride filter, or in some cases, centrifuged for 5 min at 5000 × g to remove insoluble aggregate.

Infrared spectra were recorded on a Bruker Vector 22 FTIR spectrometer (Bruker Optics, Billerica, MA), equipped with a liquid N_2-cooled photovoltaic mercury-cadmium-telluride detector, and continuously purged with dry, CO_2-free air. Unless otherwise stated, solution spectra were obtained in attenuated total reflectance (ATR) mode, using the BioATRcell II (Harrick Scientific, Pleasantville, NY) with a 4-mm-diameter multireflection silicon ATR crystal (sample volume, 7.5 μL). All spectra were obtained at room temperature. To prevent cross-contamination, after each measurement, the ATR crystal was washed with 10 sample volumes of 2 mM EDTA/2 mM EGTA, followed by buffer. All spectra are the accumulated average of 256 scans at 2-cm^{-1} resolution, with a zero-filling factor of 2 (final spectra are 1 point per cm^{-1}). Spectra were corrected for absorption of buffer and atmospheric water vapor by manually subtracting blank spectra, to obtain a flat baseline in the 1750–1850 cm^{-1} region. Because ATR spectra are known to exhibit altered peak intensity (particularly at high frequency) relative to absorption spectra (47), ATR spectra were converted to ''simulated'' absorbance-mode spectra by normalizing, using a linear function in the Opus 4.0 software program (Bruker Optics). Comparison of spectra collected in this manner with those obtained in transmission mode (using barium fluoride windows) showed no difference in band positions, indicating that anomalous dispersion effects were negligible in our experiments (data not shown). Overlaid spectra were normalized to a constant peak area from 1800–1600 cm^{-1}. Subtraction, normalization, and differentiation of spectra were performed in Opus 4.0, and graphing and fine-structure enhancement (see below) were performed using IgorPro 6 (WaveMetrics, Inc., Lake Oswego, OR). Averaged data from at least 10 separate experiments are shown. Difference spectra are the average of individual subtractions obtained from at least six experiments. As a control, error spectra were determined by separating the unaveraged difference spectra into two datasets, which were subtracted and divided by $\sqrt{2}$ to compensate for differences in average and error spectral counts (48).

Fine-structure enhancement of FTIR spectra

The principle of fine-structure enhancement (FSE), a method of identifying component peaks of broad spectral bands, was described by Barth (49). Briefly, the FSE of a spectrum S involves generating a smoothed version of S (S_{sm}), and subtracting the smoothed spectrum from the original:

$$S_{FSE} = S - WS_{sm},$$

where S_{FSE} is the final (fine structure-enhanced) spectrum, and W is a ''weighting factor'' ($0 < W < 1$). Difference spectra were smoothed over a 13-cm^{-1} window (25 data points), using a Savitsky-Golay algorithm, and the smoothed spectra were subtracted from the original spectra using a weighting factor $W = 0.985$, according to Barth (49). To verify that this procedure faithfully enhanced features present in the original absorbance spectra, the FSE procedure was also performed on the absorbance spectra (Supplementary Material, Data S1). The resulting enhanced spectra were qualitatively similar to those obtained using Fourier self-deconvolution, with a Lorentzian line and a bandwidth of 16 cm^{-1} (data not shown).

RESULTS

Oxidation-induced changes in ATR-FTIR absorbance spectra of CaM

Fourier-transform infrared spectroscopy provides a powerful tool to study the effects of Met oxidation on the backbone fold and Ca^{2+}-binding ligands of CaM. For comprehensive analysis, spectra were acquired in both D_2O and H_2O buffers, allowing greater visualization of amide and carboxylate (COO^-) stretch regions, which are resolved differently in the two solvents. The amide regions (I, II, and III, as indicated in Fig. 2, *C* and *D*) reflect peptide backbone conformations in H_2O, and these band positions are similar in D_2O (Fig. 2, *A* and *B*) with the exception of the amide II′ (deuterated amide II) peak, which downshifts to reveal antisymmetric (Asy) COO^- stretching bands near 1580 cm^{-1} (Fig. 2, *A* and *B*). Visualization of the Asy COO^- bands in D_2O provides information regarding Ca^{2+} liganding by Asp and Glu carboxylate side chains, as complemented by absorbance bands in the symmetric (Sy) COO^- stretching region (~1404 cm^{-1}) that are more readily observed in H_2O (30,36,42). The sensitivity of FTIR is apparent in the significant oxidation-induced spectral changes that reflect the effects of oxidation on the helical environment of CaM (Fig. 2, *A–D*, amide I/I′) and Ca^{2+} liganding (Fig. 2 *A*, Asy COO^-).

Upon oxidation, the greatest perturbation occurs in the Asy-COO^- region of the Ca^{2+}-bound state (Fig. 2 *A*), where the peak at 1581 cm^{-1} (CaM) downshifts to 1576 cm^{-1} (CaM_{ox}), suggesting alterations in the Asp and Glu coordination of Ca^{2+} (42,50,51). In comparison, the Asy-COO^- band of apo-CaM (Fig. 2 *B*) experiences very little shift, and retains intensity upon oxidation, indicating that the oxidation-dependent shift of Asp/Glu side-chain absorbances is specific for the Ca^{2+}-bound state. An effect by oxidation on secondary structure can be seen in a downshift of the amide I/I′ bands (~2 to 6 cm^{-1}), yet overall, retention of the α-helical protein conformation is indicated by the nominal shift in the amide III band resolved in H_2O (52–55). It is therefore evident that Met oxidation produces minimal changes in the conformation of CaM, but marked changes in the signal of side-chain carboxylate groups, suggesting an effect of oxidation on Ca^{2+}-coordinating ligands.

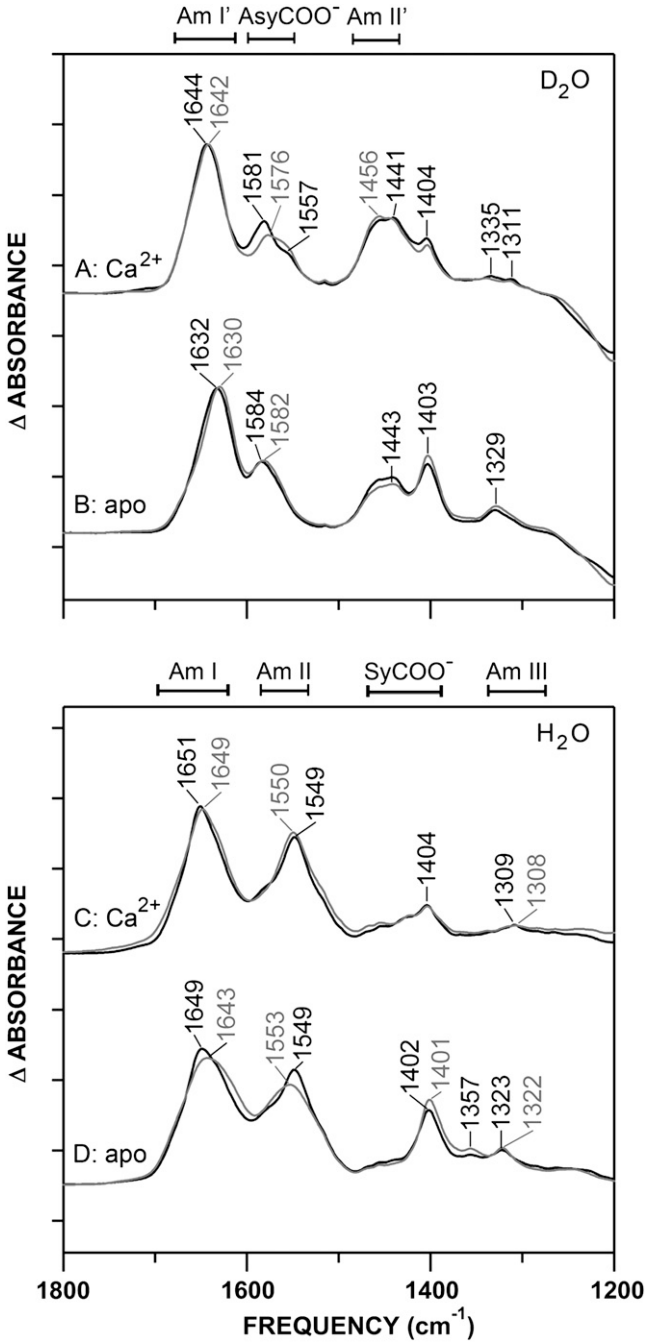

FIGURE 2 The FTIR absorbance spectra of CaM (*black*) and CaM_{ox} (*gray*) (10 mg/mL). Positions of major bands in D_2O (*A* and *B*) and H_2O (*C* and *D*) and their maxima (cm^{-1}) are indicated. Spectra were acquired in Tris buffer, pH/pD 7.5, at room temperature. Sample buffer contained 10 mM $CaCl_2$ (*A* and *C*), or samples were depleted of metals using EGTA/EDTA (*B* and *D*). Spectra were buffer-subtracted and normalized to a constant amide I/I′ band area, as described in Experimental Procedures. Tick marks on *y* axis represent Δ0.2 absorbance units.

Identification of FTIR bands associated with calcium liganding, using difference spectra

To aid in the interpretation of the oxidation effects observed in Fig. 2, we examined the Ca^{2+}-CaM minus apo-CaM difference spectrum (Fig. 3 *A*), which reflects known structural changes upon Ca^{2+} binding to CaM. To reveal further component peaks, FSE (49) and second-derivative techniques (56) were used (Fig. 3, *B–D*). Importantly, the majority of peaks observed in the FSE difference spectrum correspond to minima in second-derivative spectra, providing strong evidence that the FSE bands reflect resolved

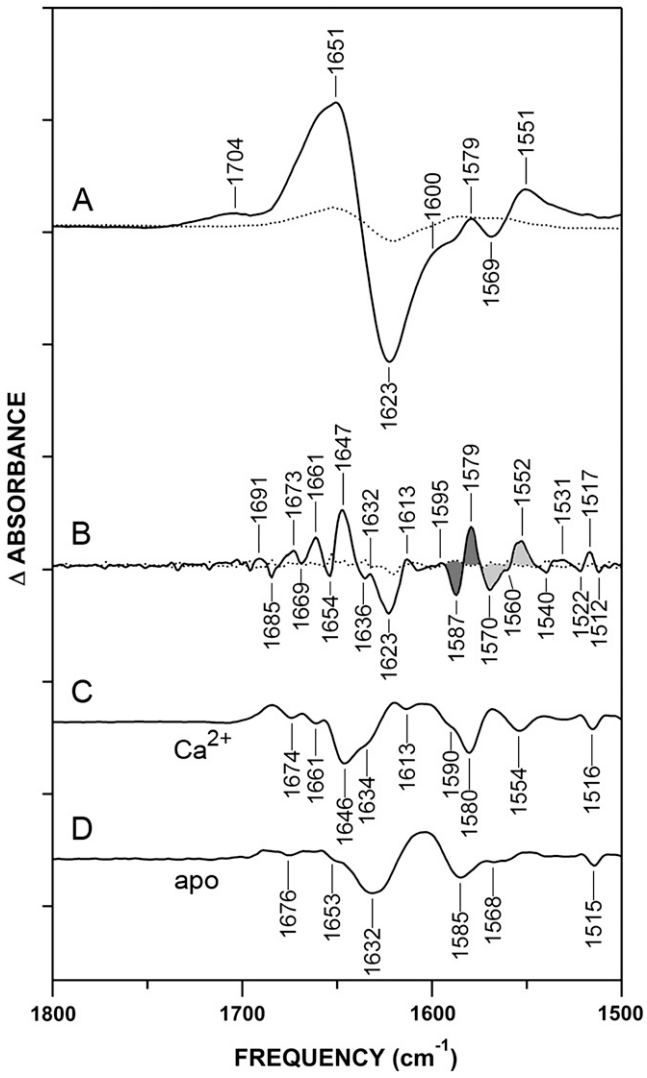

FIGURE 3 Identification of D_2O absorbance bands associated with Ca^{2+} ligands in nonoxidized CaM. (*A*) Ca^{2+}-CaM-minus-apo-CaM difference spectrum (*solid line*) and error spectrum (averaged subtractions of spectra of like samples, *dotted line*). Positive peaks reflect structures in Ca^{2+}-bound state, and negative peaks reflect structures in apo-state. (*B*) Fine structure-enhanced difference spectrum (*solid*) and error (*dotted line*), generated from *A*, as described in Experimental Procedures. Resulting spectra were multiplied by a factor of 10. Band shifts assigned to Ca^{2+}-coordinating Asp and Glu carboxylates are shaded in dark gray and light gray, respectively (see also Table 1). (*C*) Second derivative of nonoxidized Ca^{2+}-CaM and (*D*) apo-CaM absorbance spectra in Fig. 2, *A* and *B*. Resulting spectra were multiplied by a factor of 25. Minima correspond to positions of component bands in original absorbance spectra. Conditions are as described in legend of Fig. 2. Tick marks on *y* axis represent Δ0.05 absorbance units.

structural features experiencing changes between the apo and Ca^{2+}-bound states of CaM. Assignments of these bands are summarized in Table 1.

The difference spectrum in Fig. 3 *A* shows a Ca^{2+}-activated change in protein conformation in the amide I′ region and liganding in the Asy-COO^- region. The appearance of positive peaks reflects changes associated with Ca^{2+} ligation, whereas negative peaks reflect the apo structure. Increased resolution of absorbance shifts are evident in both the FSE and second-derivative spectra, indicating that the broad features in Fig. 3 *A* are a compilation of overlapping bands (Fig. 3, *B–D*). In the FSE spectra, the 1570(−)/1552(+) cm^{-1} band shift upon Ca^{2+} binding is characteristic of EF-hand proteins, and reflects the formation of a bidentate Ca^{2+} coordination by Glu^{12} in the Ca^{2+} binding sequence (41–44,57) (Fig. 3 *B*). Carboxylate bands of Asp residues involved in calcium liganding are resolved in the FSE difference spectra at 1595(+)/1587(−)/1579(+) cm^{-1} (Fig. 3 *B*). These same features are well-resolved in the FSE absorbance spectra, where a single broad feature centered at 1587 cm^{-1} in apo-CaM is split into two peaks at 1593 cm^{-1} and 1580 cm^{-1} after Ca^{2+} activation (see Fig. S1 in Data S1). The large frequency shifts after Ca^{2+} activation, apparent in both the absorbance and difference spectra, reflect the fact that 11 of 17 Asp residues in CaM function as Ca^{2+} ligands (Fig. 1).

The 1587-cm^{-1} band apparent in apo-CaM is characteristic of Asp carboxylates in the ionic (nonliganded) state (36,42, 43,58). The shift of Asp bands to both higher-frequency and lower-frequency positions upon calcium binding is indicative of two different liganding environments. The higher-frequency 1595(+) cm^{-1} peak is indicative of Asp carboxylates in a monodentate or bridging ligand structure, whereas the lower-frequency 1579(+) cm^{-1} band absorbs in a region characteristic of a weak pseudobridging interaction involving the Asp side chain, Ca^{2+}, and solvent (36,39–43). Although they were not specifically commented on, these shifts can be seen in previously reported FTIR spectra of CaM (42,51). Examination of the relative orientation and surface accessibility of the Asp side chains in the EF-hands of CaM supports the assignments of the 1595(+) cm^{-1} and 1579(+) cm^{-1} peaks (4,59) (see Discussion).

The conserved Asp^1 of the EF-loop has a lower surface accessibility than Asp^3 and Asp/Asn^5, and therefore has a greater probability of binding in either a monodentate or bridging fashion (1595(+) cm^{-1}), where the peptide backbone is the hydrogen-bonding partner (60). On the other hand, Asp^3 and Asp/Asn^5 are in close proximity to the Ca^{2+}-bound H_2O (itself bound to the side chain at position 9), creating the potential for pseudobridging interactions (1579(+) cm^{-1}) between Ca^{2+} and this water molecule. In CaM_{ox}, similar frequency shifts are observed in Ca^{2+}-minus-apo difference spectra (see Fig. S2 in Data S1), although the absorbance frequencies of the Ca^{2+}-bound Asp residues differ slightly from those in the nonoxidized protein (see below). Band shifts upon Ca^{2+} binding also occur in the Sy-COO^- region in both CaM and CaM_{ox} (see Fig. S3 in Data S1). Although we do not assign these shifts to specific binding geometries, the appearance of multiple bands at 1451, 1428, and 1411 cm^{-1} upon Ca^{2+} binding supports the presence of two populations of Ca^{2+}-bound aspartates in Ca^{2+}-CaM.

Resolution of calcium-dependent increases in helix stability

Ca^{2+} binding also produces absorbance changes in the conformation-sensitive amide I′ band of CaM. Based on high-resolution structures of CaM, it is known that Ca^{2+} binding ''opens'' the target-binding pockets (located between the central linker and the helices flanking the EF-hands) and stabilizes helices in the linker region, elongating the molecule (1). This conformational change is reflected in the gain of intensity in the α-helical region of the amide I′ band and a loss of intensity at lower frequencies (unordered and β-sheet structures). In the FSE spectrum (Fig. 3 *B*), a marked band shift upon Ca^{2+} binding can be seen at 1654(−)/1647(+) cm^{-1}. The 1654(−) cm^{-1} peak is a ''classic'' α-helical absorbance frequency, whereas the 1647(+) cm^{-1} band was previously assigned to highly solvent-exposed α-helices (61–63). This band pair therefore reflects helices that are shielded from solvent in the apo-state, and become exposed upon Ca^{2+} activation. Additional bands between 1691 cm^{-1} and 1661 cm^{-1} probably arise from the reorganization of turns

TABLE 1 Assignment of bands in fine structure-enhanced FTIR difference spectra

	Turns/β	Bent/ disordered helix	α-helix	Solvated α-helix	β-sheet	α-helix/ β-sheet interaction	Asy-COO^-, monodentate Asp	Asy-COO^-, ionic Asp	Asy-COO^-, ionic Glu	Asy-COO^-, pseudobridging Asp	Asy-COO^-, bidentate Glu	Asy-COO^-, bidentate Asp
Ca^{2+}-CaM	1673	1661	–	1647	1632	–	1707, 1593	–	–	1580	1552	–
Apo-CaM	1685	1669	1654		1636	–	–	1587	1570	–	–	–
Ca^{2+}-CaM_{ox}	1674	1660	–	1645	1631	1623	1743, 1602	–	–	1570	1552	1549
Apo-CaM_{ox}	1683	1667	1653	–	1635	1622	–	1586	1571	–	–	–
Reference for assignment	(31)	(31,58)	(31)	(58,61,63)	(31)	(65–67)	(40,41,43,78)	(43,58,78)	(43,58,78)	(78)	(41–43,78)	(78)

Positions in cm^{-1} of component bands in amide I′ and Asy-COO^- regions of fine structure-enhanced FTIR difference spectra. Assignments for Ca^{2+}-CaM and apo-CaM were based, respectively, on positive and negative peaks in FSE difference spectra of Fig. 3 *B* and Fig. S2 *B* in Data S1, except for the monodentate and pseudobridging Asp bands that were based on Fig. 4.

and bends upon Ca^{2+} binding, whereas the 1636(−)/1632(+) cm^{-1} band pair suggests a reorientation of β-structure, which is responsible for allosteric communication between neighboring EF-hands of the protein (4,64). Consistent with this assignment, a comparison of the structures of apo-CaM and Ca^{2+}-CaM reveals that the strands of these β-sheets become reoriented on Ca^{2+} binding (5,7,9,10). The broad 1623(−) cm^{-1} band, reflecting apo-CaM, occurs at a position consistent with previously described absorbances of extended chains (65,66), side chains of Arg, Tyr, or Gln residues (36), interactions between α-helices and β-sheets (67), and the intermolecular β-sheet (33,65). It is intriguing to note that evidence of interactions between the unstructured N-terminus and uncoiled central linker of apo-CaM was reported (68). The 1623(−) cm^{-1} band may reflect an intramolecular interaction by this structure that is similar in absorbance to a β-sheet/α-helix interaction. In addition, a Ca^{2+}-induced gain in intensity at 1613 cm^{-1} could be associated with changes in Arg or Tyr hydrogen bonding (36,69), suggesting that side chains also contribute to the 1623(−) cm^{-1} band.

CaM_{ox} maintains native fold, whereas Met oxidation promotes helical destabilization

In the Ca^{2+}-bound state, oxidation of CaM produces shifts in the amide I′ band, indicating that some degree of conformational change occurs upon Met oxidation (Fig. 4). The most notable of these changes is the 1650(−)/1642(+) cm^{-1} band pair, which reflects a shift of α-helical absorbance (Fig. 4 *B*). This 8-cm^{-1} downshift is comparable to that observed upon binding of Ca^{2+} (Fig. 3 *B*), strongly suggesting that it reflects an alteration in the hydration of α-helices. In fact, the oxidation of methionine residues was shown by NMR spectroscopy (16) and oxidative surface mapping (70) to induce disordering or transient unwinding of α-helices in the neighborhood of the oxidized residue, which would cause a downshift in the amide I′ absorbance frequency (61–63). We therefore attribute this band shift to the destabilization of helices induced by the oxidation of methionines. The shift to 1642 cm^{-1} could also be interpreted as a replacement of helices with an unordered structure. However, the retention of the amide III maximum at 1308/1309 cm^{-1} upon oxidation (Fig. 2 *C*, see Fig. S3 in Data S1) indicates that CaM_{ox} remains mostly helical, and that the 1650(−)/1642(+) cm^{-1} shift reflects a destabilization or transient unfolding, rather than a loss, of helices. This observation is also consistent with previous data showing that Ca^{2+} binding restores the native fold of CaM_{ox} (22,23). Other band shifts in the 1700–1658 cm^{-1} range suggest subtle rearrangements in turns and bends, whereas the 1635(−)/1629(+) cm^{-1} shift likely reflects a change in the β-sheets of CaM, possibly suggesting a different conformational preference in the EF-hands of CaM_{ox}.

In apo-CaM, the overall shift of the amide I′ region suggests some loss of helical structure upon oxidation. However,

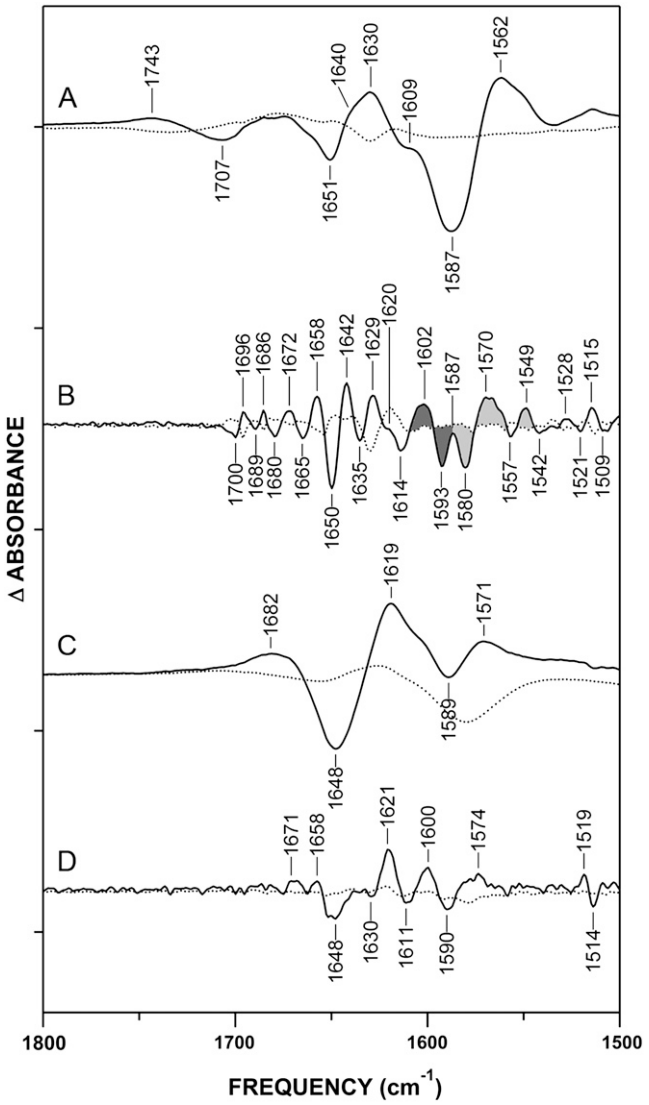

FIGURE 4 Conformational effects of oxidative modifications of CaM observed in D_2O spectra: CaM_{ox}-minus-CaM difference spectrum of Ca^{2+} activated CaM (*A* and *B*) and apo-CaM (*C* and *D*) in D_2O. (*B*) Fine-structure enhancement of *A*. Two populations of Asp residues are indicated by shading (see Results and Discussion): monodentate (*dark gray*) and pseudobridging and bidentate (*light gray*). (*C*) CaM_{ox}-minus-CaM difference spectrum of apo-CaM. (*D*) Fine-structure enhancement of *C*. In all traces, difference spectra are represented by solid lines, and error spectra by dotted lines. Fine-structure enhancement was performed as described in Experimental Procedures, and was multiplied by a factor of 25. Conditions are as described in legend of Fig. 2. Tick marks on *y* axis represent Δ0.05 absorbance units.

as in Ca^{2+}-CaM, apo-CaM retains an amide III maximum at 1322 cm^{-1}, consistent with the retention of helical structure (Fig. 2 *D*). In the FSE spectrum (Fig. 4 *D*), the band pair 1648(−)/1621(+) cm^{-1} may reflect the loss of α-helical structure by oxidation-induced unraveling of the central linker, coupled with a potential increase in interactions between the linker and the N-terminus, as proposed by Faga et al. (68). The 1621(+) cm^{-1} band may also contain contributions from the intermolecular β-sheet because of protein

aggregation (22), although precautions were taken to remove insoluble aggregate from samples before data collection (see Experimental Procedures). Further band shifts at 1671(+) cm^{-1} and 1658(+) cm^{-1} likely reflect a slight increase in turns or bent/disordered helices, either globally or in the metastable central linker helix of CaM (31,33,58).

Met oxidation alters calcium coordination by carboxylate side chains

The absorbance spectrum of Ca^{2+}-CaM_{ox} differs most noticeably from that of Ca^{2+}-CaM in the Asy-COO^- stretching region (Fig. 2 *A*). This observation suggests that Met oxidation alters the coordination of Ca^{2+} by CaM_{ox}, because the Asy-COO^- peak is sensitive to cation binding. To explore this possibility, we examined CaM_{ox}-minus-CaM difference spectra, in both the presence and absence of Ca^{2+} (Fig. 4), to investigate oxidation-dependent shifts in carboxylate absorbance. Comparison of the FSE spectra for Ca^{2+}-CaM and apo-CaM shows an increased number of oxidation-induced spectral perturbations in the Asy-COO^- region of the more rigid Ca^{2+}-bound form (Fig. 4, *B* and *D*). This finding suggests that most of the change in Asy-COO^- absorbance occurring upon Met oxidation results from perturbations of Ca^{2+}-liganding Asp/Glu residues. The Asy-COO^- shifts seen upon oxidation of apo-CaM, in contrast, likely reflect changes in solvent exposure or intramolecular interactions (e.g., salt bridging) of carboxylates not involved in Ca^{2+} binding (see below).

The prominent shifts observed in the Asy-COO^- region of the Ca^{2+}-CaM FSE difference spectra (Fig. 4 *B*) reveal two oxidation-induced band shifts at 1602(+)/1593(−)cm^{-1} and 1580(−)/1570(+) cm^{-1}, which are consistent with changes in the absorbance of Asp residues. The negative bands at 1593 cm^{-1} and 1580 cm^{-1} reflect contributions by nonoxidized CaM, and correlate with bands assigned to the two Ca^{2+} liganding populations of Asp observed in the apo-CaM spectrum (Fig. 3 *B*). Therefore, we propose that the 1580(−)/1570(+) cm^{-1} downshift results from increased stabilization of the weak pseudobridging interaction between Asp, Ca^{2+}, and solvent water formed upon Ca^{2+} binding. In addition, the 1602(+)/1593(−) cm^{-1} upshift correlates with a shift toward a stronger or more ''monodentate-like'' interaction with Ca^{2+}. This scenario likely results from a loss or weakening of hydrogen bonding between the EF-loop Asp^1 (1593(−) cm^{-1}) and the polypeptide backbone, leading to a ''pure'' monodentate coordination (1602(+) cm^{-1}) of Ca^{2+} by this Asp residue. Indeed, the FTIR spectrum of CaM saturated with Mg^{2+}, which is known to complex with EF-hands solely through monodentate coordination by aspartates (4,71), has a primary Asy-COO^- peak at 1600 cm^{-1} (data not shown), very close to the 1602-cm^{-1} peak observed in Fig. 4 *B*.

A critical ligand for maintaining Ca^{2+} coordination is the conserved glutamate residue at the twelfth position of the Ca^{2+} binding sequence (Fig. 1 *B*). In the Ca^{2+}-bound state, this residue coordinates Ca^{2+} in the bidentate mode (4,5,7,8,10), and forms hydrogen bonds with the polypeptide backbone at positions 2 and 9 of the EF-loop (72,73). These interactions are believed to be responsible for both the Ca^{2+} specificity of the EF-hands of CaM, and for the allosteric coupling between Ca^{2+} binding sites (4,71–74). According to the data in Fig. 4, the oxidation of methionines in Ca^{2+}-CaM has no apparent effect on the 1552-cm^{-1} peak associated with the Glu coordination of Ca^{2+} (Fig. 4 *B*), indicating that the bidentate coordination between Glu^{12} and Ca^{2+} is retained upon Met oxidation. This result is consistent with previous measurements indicating that the oxidation of all nine methionines to their sulfoxides does not affect the stoichiometry of Ca^{2+} binding (15). Moreover, the second-derivative spectra of both nonoxidized (Fig. 3 *C*) and oxidized (see Fig. S1 in Data S1) Ca^{2+}-CaM display a minimum at 1554 cm^{-1} and 1552 cm^{-1}, respectively, further indicating that CaM oxidation does not appreciably disrupt the bidentate coordination of Ca^{2+} by Glu residues. However, there is an absorbance increase at 1549(+) cm^{-1} that is consistent with the bidentate coordination of Ca^{2+} by a carboxylate. Molecular-dynamics simulations report that disruption of the Asp^1 interaction with the polypeptide backbone can result in a bidentate ligation of Ca^{2+} by Asp^3 (75). Therefore, it is likely that increased monodentate coordination by Asp^1 (discussed above) results in the formation of bidentate coordination by Asp^3, as indicated by a band at 1549(+) cm^{-1}.

In apo-CaM, Asy-COO^- bands are also observed, indicating that certain Asp residues undergo an oxidation-dependent absorbance shift in the absence of Ca^{2+} (Fig. 4 *D*). The band pair at 1600(+)/1590(−) cm^{-1} suggests a shift in Asp from ionic to bridging or monodentate absorbance frequencies. A potential explanation for this band shift involves the reported interaction between the N-terminal tail and the destabilized central linker of apo-CaM (68). There is a potential for further helix destabilization by oxidation of Met^{76}, which would likely alter interactions between Asp^{78} and Asp^{80} (in the central linker of CaM) and the N-terminal residues (68). The broad absorbance increase at 1574(+) may reflect changes in the environment of Glu residues and the possible formation of salt bridges that result in a broadening of absorbance (76). Upon Ca^{2+} binding, the retention of native fold by Ca^{2+}-CaM_{ox} would eliminate N-terminal interactions with the central linker. Therefore, we conclude that the majority of Asy-COO^- absorbance changes upon Ca^{2+}-CaM oxidation are related to changes in Ca^{2+} binding.

An additional 1743(+)/1707(−) cm^{-1} band pair was detected that is unique to the difference spectrum of Ca^{2+}-CaM (Fig. 4 *A*). These peaks are too broad to appear in the FSE spectrum. Bands in this region, normally associated with the C=O stretch of protonated carboxyl groups, may occur in the FTIR spectra of ionized carboxylates bound to metal ions in a monodentate mode (36,77–79). We suggest that the 1707(−) cm^{-1} band represents absorbance by the noncomplexed carbonyl of Asp^1 upon Ca^{2+} binding, reflecting a double

bond characteristic that is typical of highly asymmetric monodentate carboxylates (78,79). This scenario can be visualized as the metal cation effectively acting as a proton, pulling electron density from the coordinating oxygen to make the noncomplexed carbonyl more ''double bond-like''(78). In CaM_{ox}, a further increase in monodentate coordination would again increase the double bond characteristic of the noncoordinating carbonyl, resulting in an absorbance shift to 1743(+) cm^{-1}. Therefore, the two band shifts at 1743(+)/1707(−) cm^{-1} and 1602(+)/1593(−) cm^{-1}, together with the similarity of the 1602(+) cm^{-1} band to the Asy-COO^- band of Mg^{2+}-CaM (data not shown), lead us to propose that Met oxidation results in the loss of hydrogen-bonding interactions between the monodentate Asp^1 of certain EF-loops and the backbone, thereby strengthening the monodentate coordination of Ca^{2+} by Asp^1. Further spectral shifts can be seen in the symmetric COO^- stretching band (see Fig. S4 in Data S1). Although we do not assign shifts in this region to specific coordination structures, the oxidation-dependent loss of bands at 1452 cm^{-1} and 1432 cm^{-1} is consistent with our assignment of band shifts in two different populations of Asp residues.

In conclusion, band shifts in the Asy carboxylate-stretching band of Ca^{2+}-CaM indicate that methionine oxidation modifies the mode of Ca^{2+} coordination by carboxylate side chains in the four EF-hand binding motifs of CaM (Fig. 2). We propose that Asp residues are responsible for these results, because the critical bidentate ligation of Ca^{2+} by the conserved Glu^{12} of the Ca^{2+} binding sequence remains intact upon Met oxidation. These findings suggest that altered coordination of Ca^{2+} by Asp residues in the binding sites may underlie the order-of-magnitude decrease in apparent Ca^{2+} affinity upon oxidation of CaM methionines (15), and has the potential to explain observed disruptions in Ca^{2+} signaling under conditions of oxidative stress (26,80,81). Changes in the Asy-COO^- band upon oxidation of Ca^{2+}-CaM (Fig. 4) arise from shifts in two classes of carboxylate residues: we suggest that Asp^1 shifts to a higher frequency, whereas Asp^3 and/or Asp^5 shifts to a lower frequency (Fig. 5). We further propose that these band shifts reflect an increase in monodentate coordination by Asp^1, which may lead to bidentate Ca^{2+} ligation by Asp^3, and stabilization of a pseudobridging interaction by Asp^5.

DISCUSSION

Summary

Using FTIR spectroscopy, we resolved spectral shifts in the amide I′ and Asy-COO^- stretching bands upon oxidation of methionine in CaM, and assigned these absorbance shifts to 1), an increased solvent exposure of α-helices in CaM_{ox}; and 2), an oxidation-induced change in the coordination of Ca^{2+} by carboxylate side chains in the EF-hands of CaM. We hypothesize that the carboxylate side chains reflect two populations of Ca^{2+}-liganding Asp residues affected by CaM oxidation: one that shifts to a lower frequency (i.e., from 1580 cm^{-1} to 1570 cm^{-1} and 1549 cm^{-1}), and one that shifts to a higher frequency (i.e., from 1593 cm^{-1} to 1602 cm^{-1}; Fig. 4 *B*). In comparison, methionine oxidation does not affect the band at 1552 cm^{-1} associated with Ca^{2+}-bound glutamates. This latter result is consistent with retention of the bidentate coordination of Ca^{2+} by the conserved Glu^{12} in the Ca^{2+} binding sequence. The oxidation-induced changes in Asy-COO^- absorbance (Fig. 2) are consistent with a change in the mode of Ca^{2+} coordination by Asp ligands, i.e., Asp^1 and Asp^3/Asp^5 of the EF-loop (Fig. 1). The FTIR spectra also showed increased levels of solvent exposure of α-helical amide groups upon Met oxidation, evident as a spectral shift from 1650 cm^{-1} to 1642 cm^{-1} in amide I′ difference spectra after FSE (Fig. 4 *B*). Thus, whereas methionine oxidation results in significant spectral changes in the absorbance bands associated with carboxylates involved in Ca^{2+} liganding for Ca^{2+}-CaM, there are also important spectral changes in the amide I′ band, associated with destabilization of α-helical folds. Taken together, these ob-

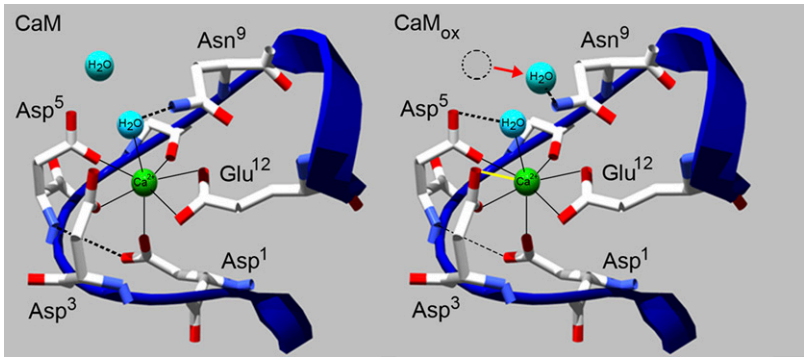

FIGURE 5 Oxidation-induced destabilization of helices in EF-hand by oxidized methionine (not shown) results in altered conformation of EF-loop that affects Ca^{2+} liganding. Alterations in Ca^{2+} liganding involve modifications in hydrogen bonding (*dashed lines*) and repositioning of a water molecule (*red arrow*) that displaces hydrogen-bonding interaction between Asn^9 and the chelating water ligand. Changes in binding involve diminished hydrogen bonding between Asp^1 and the backbone (CaM_{ox}, *thin dashed line*), apparent as an upshift in monodentate Asy COO^- absorbance from 1593(−) cm^{-1} to 1602(+) cm^{-1} (Fig. 4 *B*), which may result from destabilization of the EF-loop (not shown). This also permits the formation of a bidentate ligation of Ca^{2+} by Asp^3 (CaM_{ox}, *yellow line*), and a pseudobridging interaction between the available noncoordinating oxygen atom of Asp^5 (CaM_{ox}, *thick dashed line*), apparent as a downshift from 1580(−) cm^{-1} to 1549(+) cm^{-1} and 1580(−) cm^{-1} to 1570(+) cm^{-1}, respectively (Fig. 4 *B*). Model depicts Ca^{2+} binding site IV (1exr.pdb) (59), with generic numbering of Ca^{2+} ligands (Fig. 1) before (CaM) and after (CaM_{ox}) Met oxidation.

servations suggest that changes in the mode of Ca^{2+} coordination in CaM_{ox} can be explained by an altered conformation of the loop region of the EF-hand, caused by oxidation-induced destabilization of the helices flanking the Ca^{2+} binding sites.

Conformational changes of CaM upon methionine oxidation

The finding that oxidation of CaM increases the solvent exposure of α-helices corroborates previous results that also found Met oxidation to decrease the dynamic stability of helices and to disrupt certain tertiary-structure contacts in native CaM (16,18,19,22,24). However, these data are at odds with early measurements suggesting that the oxidation of CaM results in global unfolding, with an extensive loss of secondary structure (23). The increase in helix solvation can be interpreted in two compatible ways. In one sense, it may reflect an ''opening'' of the structure of CaM to expose otherwise solvent-shielded regions of the helix, such as that occurring upon Ca^{2+} binding (Fig. 3 *B*). This scenario is possible, but is considered unlikely, given that the α-helices of Ca^{2+}-CaM are already highly solvent-exposed in the wild-type protein before Met oxidation (5,7,51); any additional structural opening upon Met oxidation would likely be insignificant, compared with that caused by Ca^{2+} binding. Alternately, the increased solvation apparent in the amide I′ band may reflect a partial unwinding or fraying of α-helices by the presence of MetSO, a known helix-destabilizer (16,22,82). In this case, residues in a partially unwound portion of the α-helix would sample conformations similar to those of a classic helix, but with intrahelical hydrogen bonds at distorted angles and/or partially replaced by hydrogen bonds with solvent (61,62), resulting in a downshifted amide I/I′ absorbance frequency. This interpretation of the shift in the amide I′ helix signal agrees with the observed line-broadening in NMR spectra (16) and the observed loss of thermal stability of helices in CaM upon Met oxidation (22,24). Furthermore, a recent study using oxidative surface mapping (70) revealed that in apo-CaM, the reactivity of Met^{145} toward the hydroxyl radical increased after oxidation of Met^{144}, suggesting that local disordering of the polypeptide backbone occurs when Met is oxidized. Together, these findings strongly suggest that methionine oxidation induces a destabilization, but not an unfolding per se, of CaM helices in the neighborhood of Met residues.

Oxidation modifies the coordination of calcium by carboxylate side chains

The finding that Met oxidation alters the coordination of Ca^{2+} by EF-hand carboxylate side chains suggests a structural basis for the observed order-of-magnitude decrease in apparent Ca^{2+} affinity after the oxidation of CaM (15). This effect can be observed after the oxidation of as few as two vicinal C-terminal methionines adjacent to the fourth (highest-affinity) Ca^{2+} binding site of CaM (15). Our results indicate that the oxidation of methionines in CaM results in a modification of hydrogen-bond interactions of carboxylate ligands that likely involve Asp^1, which was previously associated with a loss of Ca^{2+} affinity. In troponin C, which is structurally homologous to CaM, diminished Ca^{2+} affinity is evident with the disruption of interactions between Asp^1 and the EF-loop backbone (60). Molecular-dynamics simulations of an equivalent perturbation of Asp^1 interactions in CaM revealed a rearrangement of Asp^3 coordination of Ca^{2+} from a monodentate to a bidentate mode, resulting in an additional Ca^{2+} ligand (75). This leads us to suggest that oxidation-induced destabilization of helices results in alterations in Asp coordination of Ca^{2+}, while maintaining a stable Glu bidentate coordination. Although all four Ca^{2+}-binding sites in CaM are geometrically similar (Fig. 1), the sensitivity of Ca^{2+} binding to the oxidation of CaM may, in part, be attributable to the bracketing of the EF-loop in site IV by three methionine side chains, including the functionally sensitive Met^{144}/Met^{145} (Fig. 1). Using a recent high-resolution crystal structure of Ca^{2+}-CaM (59), it is possible to construct a model of oxidation-induced perturbations in Ca^{2+} liganding, suggesting conformational rearrangements consistent with the observed spectral shifts. Although the model reflects the crystal structure of Ca^{2+} binding site IV (Fig. 5), we use generic numbering (1 through 12) for discussion of the Ca^{2+} ligands.

Two water molecules appear in the crystal structure: one that acts as a Ca^{2+} ligand, and is held in place by a hydrogen bond to the side chain $-NH_2$ of Asn^9; and a second molecule that is more distal from the cation, but that has the potential to hydrogen-bond to the Asn^9 side-chain amide group (Fig. 5, CaM). The Ca^{2+} liganding water associated with Asn^9 is also within hydrogen-bonding distance of the noncoordinating oxygen atoms of the Asp^3 and Asp^5 carboxylates (Fig. 5). Our data indicate that oxidation results in a destabilization of Met-containing helices proximal to the Ca^{2+} binding region, altering Ca^{2+} liganding. We propose that upon Met oxidation, the side-chain interaction between Asp^1 and the protein backbone is weakened, which results in the bidentate coordination of Ca^{2+} by Asp^3 (75) and the formation of a stable pseudobridging interaction between Asp^5, Ca^{2+}, and the liganding water, permitting Asp^9 to shift its interaction to the proximal water molecule (Fig. 5). This change in liganding would explain the shifts in absorbance bands from 1593 cm^{-1} to 1602 cm^{-1}, and from 1580 cm^{-1} to 1570 cm^{-1}, and the appearance of a band at 1549 cm^{-1}, which are associated with the monodentate, pseudobridging, and bidentate modes of Ca^{2+} coordination, respectively (Table 1). Spectral data also indicate that the bidentate coordination of Ca^{2+} by Glu^{12} is conserved, because there are no observed shifts in the 1552-cm^{-1} band associated with Glu coordination (Table 1).

Intriguingly, this change in coordination structure may be limited to the Asp residues of the EF-hands. The conserved

Glu residue at position 12 of the EF-hand Ca^{2+} binding sequence (Fig. 1 *B*) is known to be essential for Ca^{2+} selectivity and proper conformational change upon Ca^{2+} coordination in CaM and other EF-hand proteins (4). The fact that the bidentate coordination of Ca^{2+} by Glu^{12} is not disrupted by Met oxidation is consistent with the ability of CaM_{ox} to retain its ability to bind (but not fully activate) targets in a Ca^{2+}-sensitive manner (15,19,80). Moreover, the idea that the Asp, but not Glu, coordination of Ca^{2+} is altered by Met oxidation lends support to the hypothesis that Met oxidation disrupts CaM activation by interfering with the ordered sequence of cation binding and conformational change events necessary for proper target activation (17–19,83,84). In all EF-hands, Ca^{2+} binding is thought to occur first at the ligands at the N-terminus of the EF-loop (Asp residues in this case), followed by a ''wrapping'' of the EF-loop around the ion, terminating in the formation of bidentate coordination by Glu^{12} (72,85). A difference in the preferred coordination structure by Asp residues (i.e., by the N-terminal part of the EF-hand) may slow or otherwise interfere with the early stages of this process, altering the proper sequence of binding and conformational changes needed for proper CaM activation. Consistent with this hypothesis, previous measurements found that the oxidation of methionines in CaM disrupts the cooperativity between Ca^{2+} binding sites (15).

Our model of selective modulation of Ca^{2+} binding by Asp residues provides a conceptually interesting means of modulating the Ca^{2+} activation of sensor proteins such as CaM, because the oxidation of Met is reversible through the action of methionine sulfoxide reductases, and is known to regulate Ca^{2+} signaling under conditions of oxidative stress (11,26,80). It is known that a loss of Ca^{2+} coordination by the critical Glu residue effectively abolishes the function of EF-hand proteins (4,73). By allowing this interaction to be retained, Met oxidation of CaM can modulate the function of the protein in a subtle manner, by affecting its affinity for Ca^{2+} and its relative efficacy at activating targets. The fact that the subtle conformational and cation-binding alterations induced by Met oxidation do not completely abolish the function of CaM, or cause a catastrophic unfolding or aggregation, may explain why this regulatory modification of CaM appears to have persisted through evolution (11) and may be harnessed in some organisms to blunt Ca^{2+} signaling under conditions of oxidative stress (26). Particularly interesting in this regard may be the role of CaM_{ox} in the cellular response to ionizing radiation, which is known both to stimulate Ca^{2+} signaling and to generate reactive oxygen/nitrogen species (25,27,28); experiments aimed at defining this role are underway in our laboratory. The observation that the oxidative modification of CaM can affect its metal-binding propensity, furthermore, suggests that fine-tuning cation coordination in a metal-binding protein may be a particularly useful way to modulate its function. Sensitivity to such modifications may be a common feature of metal-binding proteins subject to posttranslational regulation in vivo.

CONCLUSIONS AND FUTURE DIRECTIONS

We demonstrated that the oxidation of methionines in CaM selectively alters the coordination of the Ca^{2+} ion by the carboxylate side chains in the EF-hand binding clefts. We propose that oxidation differentially modifies Ca^{2+} liganding by two populations of Asp residues, acting to weaken the hydrogen-bond interaction between Asp^{1} and the EF-loop, and to alter selectively the mode of binding interactions between Asp^{3} and Asp^{5} and Ca^{2+}. The overall result is to diminish effectively the Ca^{2+} binding affinity of CaM_{ox}. These findings support the role of destabilized structure and the disruption of tertiary contacts in the inactivation of CaM by oxidation, and further suggest that altered Ca^{2+} liganding may play a role in the nonproductive association of CaM with a range of target proteins, resulting in large reductions in their function. Future measurements should be directed at resolving residue-specific changes in binding interactions at individual Ca^{2+} binding sites in CaM, and their effects on both cooperative calcium binding and the mechanism of target-protein association with CaM_{ox}.

SUPPLEMENTARY MATERIAL

To view all of the supplemental files associated with this article, visit www.biophysj.org.

We thank Drs. D. Bigelow and N. Karin for helpful discussions, Dr. H. Smallwood and Mr. M. Jacoby for the initial purification of calmodulin, and Ms. S. B. Reed for providing Milli-Q deionized water.

This research was supported by a grant from the Low Dose Radiation Research Program, Office of Biological and Environmental Research, United States Department of Energy. Pacific Northwest National Laboratory (PNNL) is operated for the Department of Energy by the Battelle Memorial Institute under contract DE-AC06-76RL0 1830.

REFERENCES

1. Chin, D., and A. R. Means. 2000. Calmodulin: a prototypical calcium sensor. *Trends Cell Biol.* 10:322–328.
2. Clapham, D. E. 2007. Calcium signaling. *Cell.* 131:1047–1058.
3. Yap, K. L., J. Kim, K. Truong, M. Sherman, T. Yuan, and M. Ikura. 2000. Calmodulin target database. *J. Struct. Funct. Genomics.* 1:8–14.
4. Gifford, J. L., M. P. Walsh, and H. J. Vogel. 2007. Structures and metal-ion-binding properties of the Ca^{2+}-binding helix-loop-helix EF-hand motifs. *Biochem. J.* 405:199–221.
5. Babu, Y. S., C. E. Bugg, and W. J. Cook. 1988. Structure of calmodulin refined at 2.2 Å resolution. *J. Mol. Biol.* 204:191–204.
6. Babu, Y. S., J. S. Sack, T. J. Greenhough, C. E. Bugg, A. R. Means, and W. J. Cook. 1985. Three-dimensional structure of calmodulin. *Nature.* 315:37–40.
7. Chattopadhyaya, R., W. E. Meador, A. R. Means, and F. A. Quiocho. 1992. Calmodulin structure refined at 1.7 Å resolution. *J. Mol. Biol.* 228:1177–1192.

8. Chou, J. J., S. Li, C. B. Klee, and A. Bax. 2001. Solution structure of Ca^{2+}-calmodulin reveals flexible hand-like properties of its domains. *Nat. Struct. Biol.* 8:990–997.
9. Kuboniwa, H., N. Tjandra, S. Grzesiek, H. Ren, C. B. Klee, and A. Bax. 1995. Solution structure of calcium-free calmodulin. *Nat. Struct. Biol.* 2:768–776.
10. Zhang, M., T. Tanaka, and M. Ikura. 1995. Calcium-induced conformational transition revealed by the solution structure of apo calmodulin. *Nat. Struct. Biol.* 2:758–767.
11. Bigelow, D. J. and T. C. Squier. 2005. Redox modulation of cellular signaling and metabolism through reversible oxidation of methionine sensors in calcium regulatory proteins. *Biochim. Biophys. Acta Proteins Proteomics.* 1703:121–134.
12. Gagnon, C., S. Kelly, V. Manganiello, M. Vaughan, C. Odya, W. Strittmatter, A. Hoffman, and F. Hirata. 1981. Modification of calmodulin function by enzymatic carboxylic methylation. *Nature.* 291:515–516.
13. Johnson, B. A., J. M. Shirokawa, and D. W. Aswad. 1989. Deamidation of calmodulin at neutral and alkaline pH: quantitative relationships between ammonia loss and the susceptibility of calmodulin to modification by protein carboxyl methyltransferase. *Arch. Biochem. Biophys.* 268:276–286.
14. Murtaugh, T. J., L. S. Wright, and F. L. Siegel. 1986. Posttranslational modification of calmodulin in rat brain and pituitary. *J. Neurochem.* 47:164–172.
15. Yao, Y., D. Yin, G. S. Jas, K. Kuczera, T. D. Williams, C. Schoneich, and T. C. Squier. 1996. Oxidative modification of a carboxyl-terminal vicinal methionine in calmodulin by hydrogen peroxide inhibits calmodulin-dependent activation of the plasma membrane Ca-ATPase. *Biochemistry.* 35:2767–2787.
16. Anbanandam, A., R. J. Bieber Urbauer, R. K. Bartlett, H. S. Smallwood, T. C. Squier, and J. L. Urbauer. 2005. Mediating molecular recognition by methionine oxidation: conformational switching by oxidation of methionine in the carboxyl-terminal domain of calmodulin. *Biochemistry.* 44:9486–9496.
17. Bartlett, R. K., R. J. Bieber Urbauer, A. Anbanandam, H. S. Smallwood, J. L. Urbauer, and T. C. Squier. 2003. Oxidation of Met^{144} and Met^{145} in calmodulin blocks calmodulin dependent activation of the plasma membrane Ca-ATPase. *Biochemistry.* 42:3231–3238.
18. Chen, B., M. U. Mayer, and T. C. Squier. 2005. Structural uncoupling between opposing domains of oxidized calmodulin underlies the enhanced binding affinity and inhibition of the plasma membrane Ca-ATPase. *Biochemistry.* 44:4737–4747.
19. Gao, J., Y. Yao, and T. C. Squier. 2001. Oxidatively modified calmodulin binds to the plasma membrane Ca-ATPase in a nonproductive and conformationally disordered complex. *Biophys. J.* 80: 1791–1801.
20. Robison, A. J., D. G. Winder, R. J. Colbran, and R. K. Bartlett. 2007. Oxidation of calmodulin alters activation and regulation of CaMKII. *Biochem. Biophys. Res. Commun.* 356:97–101.
21. Ferrington, D. A., H. Sun, K. K. Murray, J. Costa, T. D. Williams, D. J. Bigelow, and T. C. Squier. 2001. Selective degradation of oxidized calmodulin by the 20 S proteasome. *J. Biol. Chem.* 276:937–943.
22. Gao, J., D. H. Yin, Y. Yao, H. Sun, Z. Qin, C. Schoneich, T. D. Williams, and T. C. Squier. 1998. Loss of conformational stability in calmodulin upon methionine oxidation. *Biophys. J.* 74:1115–1134.
23. Lafitte, D., P. O. Tsvetkov, F. Devred, R. Toci, F. Barras, C. Briand, A. A. Makarov, and J. Haiech. 2002. Cation binding mode of fully oxidised calmodulin explained by the unfolding of the apostate. *Biochim. Biophys. Acta: Proteins Proteomics.* 1600:105–110.
24. Sacksteder, C. A., J. E. Whittier, Y. Xiong, J. Li, N. A. Galeva, M. E. Jacoby, S. O. Purvine, T. D. Williams, M. C. Rechsteiner, D. J. Bigelow, and T. C. Squier. 2006. Tertiary structural rearrangements upon oxidation of methionine145 in calmodulin promotes targeted proteasomal degradation. *Biophys. J.* 91:1480–1493.
25. Du, Y. C., S. Gu, J. Zhou, T. Wang, H. Cai, M. A. Macinnes, E. M. Bradbury, and X. Chen. 2006. The dynamic alterations of H2AX complex during DNA repair detected by a proteomic approach reveal the critical roles of Ca^{2+}/calmodulin in the ionizing radiation-induced cell cycle arrest. *Mol. Cell. Proteomics.* 5:1033–1044.
26. Gao, J., D. Yin, Y. Yao, T. D. Williams, and T. C. Squier. 1998. Progressive decline in the ability of calmodulin isolated from aged brain to activate the plasma membrane Ca-ATPase. *Biochemistry.* 37:9536–9548.
27. Mikkelsen, R. B., and P. Wardman. 2003. Biological chemistry of reactive oxygen and nitrogen and radiation-induced signal transduction mechanisms. *Oncogene.* 22:5734–5754.
28. Hallahan, D. E., D. Bleakman, S. Virudachalam, D. Lee, D. Grdina, D. W. Kufe, and R. R. Weichselbaum. 1994. The role of intracellular calcium in the cellular response to ionizing radiation. *Radiat. Res.* 138:392–400.
29. Schallreuter, K. U., N. C. Gibbons, C. Zothner, M. M. Abou Elloof, and J. M. Wood. 2007. Hydrogen peroxide-mediated oxidative stress disrupts calcium binding on calmodulin: more evidence for oxidative stress in vitiligo. *Biochem. Biophys. Res. Commun.* 360:70–75.
30. Barth, A. 2007. Infrared spectroscopy of proteins. *Biochim. Biophys. Acta Bioenerg.* 1767:1073–1101.
31. Byler, D. M., and H. Susi. 1986. Examination of the secondary structure of proteins by deconvolved FTIR spectra. *Biopolymers.* 25: 469–487.
32. Krimm, S., and J. Bandekar. 1986. Vibrational spectroscopy and conformation of peptides, polypeptides, and proteins. *Adv. Protein Chem.* 38:181–364.
33. Surewicz, W. K., and H. H. Mantsch. 1988. New insight into protein secondary structure from resolution-enhanced infrared spectra. *Biochim. Biophys. Acta.* 952:115–130.
34. Susi, H., and D. M. Byler. 1986. Resolution-enhanced Fourier transform infrared spectroscopy of enzymes. *Methods Enzymol.* 130:290–311.
35. Venyaminov, S., and N. N. Kalnin. 1990. Quantitative IR spectrophotometry of peptide compounds in water (H_2O) solutions. II. Amide absorption bands of polypeptides and fibrous proteins in alpha-, beta-, and random coil conformations. *Biopolymers.* 30:1259–1271.
36. Barth, A. 2000. The infrared absorption of amino acid side chains. *Prog. Biophys. Mol. Biol.* 74:141–173.
37. Barth, A., and C. Zscherp. 2002. What vibrations tell us about proteins. *Q. Rev. Biophys.* 35:369–430.
38. Venyaminov, S., and N. N. Kalnin. 1990. Quantitative IR spectrophotometry of peptide compounds in water (H_2O) solutions. I. Spectral parameters of amino acid residue absorption bands. *Biopolymers.* 30:1243–1257.
39. Mizuguchi, M., M. Nara, K. Kawano, and K. Nitta. 1997. FT-IR study of the Ca^{2+}-binding to bovine alpha-lactalbumin. Relationships between the type of coordination and characteristics of the bands due to the Asp COO^- groups in the Ca^{2+}-binding site. *FEBS Lett.* 417:153–156.
40. Mizuguchi, M., M. Nara, Y. Ke, K. Kawano, T. Hiraoki, and K. Nitta. 1997. Fourier-transform infrared spectroscopic studies on the coordination of the side-chain COO^- groups to Ca^{2+} in equine lysozyme. *Eur. J. Biochem.* 250:72–76.
41. Nara, M., H. Morii, F. Yumoto, H. Kagi, and M. Tanokura. 2006. Fourier transform infrared spectroscopic study on the Ca^{2+} -bound coordination structures of synthetic peptide analogues of the calcium-binding site III of troponin C. *Biopolymers.* 82:339–343.
42. Nara, M., M. Tanokura, T. Yamamoto, and M. Tasumi. 1995. A comparative study of the binding effects of Mg^{2+}, Ca^{2+}, Sr^{2+}, and Cd^{2+} on calmodulin by Fourier-transform infrared spectroscopy. *Biospectroscopy.* 1:47–54.
43. Nara, M., M. Tasumi, M. Tanokura, T. Hiraoki, M. Yazawa, and A. Tsutsumi. 1994. Infrared studies of interaction between metal ions and Ca^{2+}-binding proteins. Marker bands for identifying the types of coordination of the side-chain COO^- groups to metal ions in pike parvalbumin (pI = 4.10). *FEBS Lett.* 349:84–88.

44. Nara, M., F. Yumoto, K. Nagata, M. Tanokura, H. Kagi, T. Ojima, and K. Nishita. 2004. Fourier transform infrared spectroscopic study on the binding of Mg^{2+} to a mutant Akazara scallop troponin C (E142Q). *Biopolymers.* 74:77–81.

45. Strasburg, G. M., M. Hogan, W. Birmachu, D. D. Thomas, and C. F. Louis. 1988. Site-specific derivatives of wheat germ calmodulin. Interactions with troponin and sarcoplasmic reticulum. *J. Biol. Chem.* 263:542–548.

46. Lasch, P., T. Petras, O. Ullrich, J. Backmann, D. Naumann, and T. Grune. 2001. Hydrogen peroxide-induced structural alterations of RNAse A. *J. Biol. Chem.* 276:9492–9502.

47. van de Weert, M., P. I. Haris, W. E. Hennink, and D. J. A. Crommelin. 2001. Fourier transform infrared spectrometric analysis of protein conformation: effect of sampling method and stress factors. *Anal. Biochem.* 297:160–169.

48. Sacksteder, C. A., S. L. Bender, and B. A. Barry. 2005. Role for bound water and CH-pi aromatic interactions in photosynthetic electron transfer. *J. Am. Chem. Soc.* 127:7879–7890.

49. Barth, A. 2000. Fine-structure enhancement—assessment of a simple method to resolve overlapping bands in spectra. *Spectrochim. Acta. A Mol. Biomol. Spectrosc.* 56:1223–1232.

50. Rainteau, D., C. Wolf, and F. Lavialle. 1989. Effects of calcium and calcium analogs on calmodulin: a Fourier transform infrared and electron spin resonance investigation. *Biochim. Biophys. Acta.* 1011:81–87.

51. Trewhella, J., W. K. Liddle, D. B. Heidorn, and N. Strynadka. 1989. Calmodulin and troponin C structures studied by Fourier transform infrared spectroscopy: effects of Ca^{2+} and Mg^{2+} binding. *Biochemistry.* 28:1294–1301.

52. Anderle, G., and R. Mendelsohn. 1987. Thermal denaturation of globular proteins. Fourier transform-infrared studies of the amide III spectral region. *Biophys. J.* 52:69–74.

53. Cai, S., and B. R. Singh. 2004. A distinct utility of the amide III infrared band for secondary structure estimation of aqueous protein solutions using partial least squares methods. *Biochemistry.* 43:2541–2549.

54. Fu, F. N., D. B. DeOliveira, W. R. Trumble, H. K. Sarkar, and B. R. Singh. 1994. Secondary structure estimation of proteins using the amide III region of Fourier transform infrared spectroscopy: application to analyze calcium-binding-induced structural changes in calsequestrin. *Appl. Spectrosc.* 48:1432–1441.

55. Seaton, B. A., J. F. Head, R. C. Lord, and G. A. Petsko. 1983. Studies of calmodulin structure—laser Raman-spectroscopy of biomolecules. *Biochemistry.* 22:973–978.

56. Susi, H., and D. M. Byler. 1983. Protein structure by Fourier transform infrared spectroscopy: second derivative spectra. *Biochem. Biophys. Res. Commun.* 115:391–397.

57. Ozawa, T., M. Fukuda, M. Nara, A. Nakamura, Y. Komine, K. Kohama, and Y. Umezawa. 2000. How can Ca^{2+} selectively activate recoverin in the presence of Mg^{2+}? Surface plasmon resonance and FT-IR spectroscopic studies. *Biochemistry.* 39:14495–14503.

58. Jackson, M., P. I. Haris, and D. Chapman. 1991. Fourier transform infrared spectroscopic studies of Ca^{2+}-binding proteins. *Biochemistry.* 30:9681–9686.

59. Wilson, M. A., and A. T. Brunger. 2000. The 1.0 Å crystal structure of Ca^{2+}-bound calmodulin: an analysis of disorder and implications for functionally relevant plasticity. *J. Mol. Biol.* 301:1237–1256.

60. Babu, A., H. Su, Y. J. Ryu, and J. Gulati. 1992. Determination of residue specificity in the EF-hand of troponin-C for Ca^{2+} coordination, by genetic-engineering. *J. Biol. Chem.* 267:15469–15474.

61. Manas, E. S., Z. Getahun, W. W. Wright, W. F. DeGrado, and J. M. Vanderkooi. 2000. Infrared spectra of amide groups in alpha-helical proteins: evidence for hydrogen bonding between helices and water. *J. Am. Chem. Soc.* 122:9883–9890.

62. Reisdorf, W. C., Jr., and S. Krimm. 1996. Infrared amide I′ band of the coiled coil. *Biochemistry.* 35:1383–1386.

63. Walsh, S. T., R. P. Cheng, W. W. Wright, D. O. Alonso, V. Daggett, J. M. Vanderkooi, and W. F. DeGrado. 2003. The hydration of amides in helices: a comprehensive picture from molecular dynamics, IR, and NMR. *Protein Sci.* 12:520–531.

64. Marchand, S., and B. Roux. 1998. Molecular dynamics study of calbindin D9k in the apo and singly and doubly calcium-loaded states. *Proteins.* 33:265–284.

65. Georget, D. M., and P. S. Belton. 2006. Effects of temperature and water content on the secondary structure of wheat gluten studied by FTIR spectroscopy. *Biomacromolecules.* 7:469–475.

66. Chehin, R., I. Iloro, M. J. Marcos, E. Villar, V. L. Shnyrov, and J. L. Arrondo. 1999. Thermal and pH-induced conformational changes of a beta-sheet protein monitored by infrared spectroscopy. *Biochemistry.* 38:1525–1530.

67. Arrondo, J. L., and F. M. Goni. 1999. Structure and dynamics of membrane proteins as studied by infrared spectroscopy. *Prog. Biophys. Mol. Biol.* 72:367–405.

68. Faga, L. A., B. R. Sorensen, W. S. VanScyoc, and M. A. Shea. 2003. Basic interdomain boundary residues in calmodulin decrease calcium affinity of sites I and II by stabilizing helix-helix interactions. *Proteins.* 50:381–391.

69. Takahashi, R., and T. Noguchi. 2007. Criteria for determining the hydrogen-bond structures of a tyrosine side chain by Fourier transform infrared spectroscopy: density functional theory analyses of model hydrogen-bonded complexes of p-cresol. *J. Phys. Chem. B.* 111: 13833–13844.

70. Sharp, J. S., and K. B. Tomer. 2007. Analysis of the oxidative damage-induced conformational changes of apo- and holocalmodulin by dose-dependent protein oxidative surface mapping. *Biophys. J.* 92: 1682–1692.

71. Ohki, S., M. Ikura, and M. Zhang. 1997. Identification of Mg^{2+}-binding sites and the role of Mg^{2+} on target recognition by calmodulin. *Biochemistry.* 36:4309–4316.

72. Evenas, J., A. Malmendal, E. Thulin, G. Carlstrom, and S. Forsen. 1998. Ca^{2+} binding and conformational changes in a calmodulin domain. *Biochemistry.* 37:13744–13754.

73. Evenas, J., E. Thulin, A. Malmendal, S. Forsen, and G. Carlstrom. 1997. NMR studies of the E140Q mutant of the carboxy-terminal domain of calmodulin reveal global conformational exchange in the Ca^{2+}-saturated state. *Biochemistry.* 36:3448–3457.

74. Evenas, J., S. Forsen, A. Malmendal, and M. Akke. 1999. Backbone dynamics and energetics of a calmodulin domain mutant exchanging between closed and open conformations. *J. Mol. Biol.* 289:603–617.

75. Likić, V. A., E. E. Strehler, and P. R. Gooley. 2003. Dynamics of Ca^{2+}-saturated calmodulin D129N mutant studied by multiple molecular dynamics simulations. *Protein Sci.* 12:2215–2229.

76. Muga, A., W. K. Surewicz, P. T. Wong, H. H. Mantsch, V. K. Singh, and T. Shinohara. 1990. Structural studies with the uveopathogenic peptide M derived from retinal S-antigen. *Biochemistry.* 29:2925–2930.

77. Deacon, G. B., and R. J. Phillips. 1980. Relationships between the carbon-oxygen stretching frequencies of carboxylato complexes and the type of carboxylate coordination. *Coord. Chem. Rev.* 33:227–250.

78. Nara, M., H. Torii, and M. Tasumi. 1996. Correlation between the vibrational frequencies of the carboxylate group and the types of its coordination to a metal ion: an ab initio molecular orbital study. *J. Phys. Chem.* 100:19812–19817.

79. Tackett, J. E. 1989. FT-IR characterization of metal acetates in aqueous-solution. *Appl. Spectrosc.* 43:483–489.

80. Sun, H., J. Gao, D. A. Ferrington, H. Biesiada, T. D. Williams, and T. C. Squier. 1999. Repair of oxidized calmodulin by methionine sulfoxide reductase restores ability to activate the plasma membrane Ca-ATPase. *Biochemistry.* 38:105–112.

81. Yin, D., K. Kuczera, and T. C. Squier. 2000. The sensitivity of carboxyl-terminal methionines in calmodulin isoforms to oxidation by

H_2O_2 modulates the ability to activate the plasma membrane Ca-ATPase. *Chem. Res. Toxicol.* 13:103–110.

82. Liu, D., D. Ren, H. Huang, J. Dankberg, R. Rosenfeld, M. J. Cocco, L. Li, D. N. Brems, and R. L. Remmele, Jr. 2008. Structure and stability changes of human IgG1 Fc as a consequence of methionine oxidation. *Biochemistry.* 47:5088–5100.
83. Boschek, C. B., T. E. Jones, H. S. Smallwood, T. C. Squier, and D. J. Bigelow. 2008. Loss of the calmodulin-dependent inhibition of the RyR1 calcium release channel upon oxidation of methionines in calmodulin. *Biochemistry.* 47:131–142.
84. Sun, H., and T. C. Squier. 2000. Ordered and cooperative binding of opposing globular domains of calmodulin to the plasma membrane Ca-ATPase. *J. Biol. Chem.* 275:1731–1738.
85. Kobayashi, C., and S. Takada. 2006. Protein grabs a ligand by extending anchor residues: molecular simulation for Ca^{2+} binding to calmodulin loop. *Biophys. J.* 90:3043–3051.
86. Kretsinger, R. H., and C. D. Barry. 1975. The predicted structure of the calcium-binding component of troponin. *Biochim. Biophys. Acta.* 405: 40–52.